AIAA 2002-2477

Trailing Edge Noise Prediction Based on a New Acoustic Formulation

J. Casper and F. Farassat
NASA Langley Research Center
Hampton, VA

8th AIAA/CEAS Aeroacoustics Conference and Exhibit
June 17-19, 2002 / Breckenridge, CO

For permission to copy or republish, contact the copyright owner named on the first page. For AIAA-held copyright, write to AIAA Permissions Department, 1801 Alexander Bell Drive, Suite 500, Reston, VA 20191-4344.

TRAILING EDGE NOISE PREDICTION BASED ON A NEW ACOUSTIC FORMULATION[1]

J. Casper* and F. Farassat†
NASA Langley Research Center
Hampton, VA 23681

Abstract

A new analytic result in acoustics called "Formulation 1B," proposed by Farassat, is used to compute broadband trailing edge noise from an unsteady surface pressure distribution on a thin airfoil in the time domain. This formulation is a new solution of the Ffowcs Williams-Hawkings equation with the loading source term, and has been shown in previous research to provide time domain predictions of broadband noise that are in excellent agreement with experiment. Furthermore, this formulation lends itself readily to rotating reference frames and statistical analysis of broadband trailing edge noise. Formulation 1B is used to calculate the far field noise radiated from the trailing edge of a NACA 0012 airfoil in low Mach number flows, using both analytical and experimental data on the airfoil surface. The results are compared to analytical results and experimental measurements that are available in the literature. Good agreement between predictions and measurements is obtained.

Nomenclature

b = airfoil semi-span (m)
C = airfoil chord (m)
c_0 = ambient sound speed (m/sec)
f = frequency (Hz)
$\tilde{f}$ = geometry function for airfoil surface (Fig. 1)
E^* = combination of Fresnel integrals (Eq. (2c))
g = surface pressure transfer function
k_c = ω/U_c, convective wave number (m^{-1})
ℓ_2 = spanwise correlation length (m)
$\vec{M}$ = $\vec{V}/c_0$, Mach number vector
M_r = $\vec{M}\cdot\vec{r}/r$ Mach number in radiation direction
M_ν = $\vec{M}\cdot\hat{\nu}$ Mach number in direction of $\hat{\nu}$
ΔP = unsteady airfoil surface pressure jump (Pa)
p = unsteady airfoil surface pressure (Pa)
p' = sound pressure radiated to observer (Pa)
$\partial p/\partial s$ = surface pressure gradient in the direction of $\vec{V}$
q_0 = $\rho_0 U^2/2$, dynamic head (kg-m/s^2)
$\vec{r}$ = $\vec{x}-\vec{y}$, sound radiation vector (m)
S_{qq} = surface pressure correlation function
T = $1/f$, acoustic period (sec)
t = observer time (sec)
U = uniform freestream speed (m/sec)
u = unsteady streamwise velocity (m/sec)
$\vec{V}$ = airfoil velocity vector
$\vec{x}$ = $[x_1, x_2, x_3]^T$, observer position
$\vec{y}$ = $[y_1, y_2, 0]^T$, surface source position
β = $\sqrt{1-M^2}$
λ = c_0/f, acoustic wave-length (m)
μ = $M\omega/\beta^2 U$
ψ = directivity angle (Fig. 4)
$\hat{\nu}$ = unit inward facing normal on surface edge (Fig. 1)
θ = angle between surface normal and $\vec{r}$ (Fig. 1)
ρ_0 = ambient density (kg/m^3)
τ = $t - r/c_0$, source time (sec)
Φ_{PP} = power spectral density of surface pressure
ϕ = random phase variable (radians)
ω = $2\pi f$, circular frequency (radians/sec)

Subscripts
$1, 2, 3$ = Cartesian coordinate directions (Fig. 2)
ret = evaluated at source time τ

1. Introduction

Trailing edge (TE) noise has been the subject of extensive research within the aeroacoustic community for decades, both experimentally and analytically. Areas of current research include the prediction of TE noise from rotating machinery and airframes. Research in the area of TE noise prediction has, in large part, been motivated by the desire to incorporate the results of TE noise analysis into a design methodology. The present work is similarly motivated, and the resulting formulation should lend itself well to an engineering design tool suite when aeroacoustics plays a role in the design.

The literature abounds with various theoretical approaches to the prediction of TE noise. Howe[1] categorized the various theories of TE noise into three groups:

(*i*) Theories based on the Lighthill[2] acoustic analogy, e.g., Ffowcs Williams and Hall[3].

(*ii*) Theories based on the solution of special problems approximated by the linearized hydrodynamics equations, e.g., Amiet[4,5] and Goldstein[6].

(*iii*) Ad hoc models, involving postulated source distributions whose strengths and types are empirically determined.

The present work falls into the first category. This

Copyright © 2002 by the American Institute of Aeronautics and Astronautics, Inc. No copyright is asserted in the United States under Title 17, U.S. Code. The U.S. Government has a royalty-free license to exercise all rights under the copyright claimed herein for Governmental Purposes. All other rights are reserved by the copyright owner.

[1] This manuscript has been revised since its original presentation. Last revision July 19, 2002.

* Research Scientist, Computational Modeling and Simulation Branch, AIAA Senior Member

† Senior Research Scientist, Aeroacoustics Branch, AIAA Assoc. Fellow

new result, "Formulation 1B," is a solution of the loading source term of the Ffowcs Williams-Hawkings equation.[7] Such time domain methods provide for a total decoupling of the acoustic signal from the aerodynamics. As such, these methods readily avail themselves to acoustic predictions that are based on input from experimental measurements or computational fluid dynamics (CFD) solutions. For example, Singer *et al*,[8] used a solution of the Ffowcs Williams-Hawkings equation to predict TE noise from sources that were modeled with CFD simulations. The acoustic formulation in their work[8] is known as "Formulation 1A."[9] What distinguishes Formulation 1B from this prior formulation is its relative simplicity, which makes it highly suitable for rotational reference frames and statistical analysis of broadband TE noise.

In Ref. 10, Formulation 1B was applied to the prediction of far field noise due to incident turbulence on a NACA 0012 airfoil at tunnel speeds ranging from 40 m/s to 165 m/s, and compared to the experimental results of Paterson and Amiet.[11] The time dependent surface pressure required as input to Formulation 1B was generated by stochastic modeling of the incident turbulence and approximation of the airfoil response with a result from thin airfoil theory. Formulation 1B was then used to predict the acoustic pressure as a function in time at a prescribed microphone location. The time domain results were then Fourier analyzed to determine the spectral density of the far field noise. The far field spectra were found to be in excellent agreement with the frequency domain predictions and experimental measurements of Paterson and Amiet[11].

The time domain approach that is described in Ref. 10 is used in the current work to predict far field radiation from the trailing edge of an airfoil. In the following section, Formulation 1B is briefly reviewed for the case of a flat surface in a general non-uniform motion. (For a formal derivation, see Ref. 10.) Some advantages of this new formulation relative to other solutions of the Ffowcs Williams-Hawkings equation are described.

In Section 3, a model problem is considered in which an unsteady surface pressure that is comprised of a single frequency induces an acoustic source at the trailing edge of a flat plate in uniform motion. The unsteady surface pressure is an analytical result from thin airfoil theory that is taken from the work of Amiet.[4,5,12] Two simple test cases are presented for validation purposes. The directivity of the tone induced by this surface pressure is examined for qualitative correctness. The results of a velocity scaling exercise are shown to be consistent with the results of Ffowcs Williams and Hall.[3]

In Section 4, the surface pressure formulation introduced in Section 3 is used as the basis function of a linear superposition that provides an analytic source model for broadband TE noise. This stochastically modeled surface pressure is used as input to Formulation 1B to predict broadband TE noise from a NACA 0012 airfoil in a low-turbulence uniform mean flow. The surface pressure correlations that are required in the aerodynamic model are taken from two sources: an empirical flat plate formulation[13,14] and experimental data.[15] The resulting calculations are compared to the acoustic predictions of Schlinker and Amiet[16] and the experimental measurements of Brooks and Hodgson.[17]

2. Acoustic Formulation

Consider a flat, finite surface moving in the plane $x_3 = 0$ along a velocity vector $\vec{V}$. The velocity vector and the plate's geometry are related to the coordinate axes as pictured in Fig. 1. Let $\tilde{f}(x_1, x_2, t)$ denote a geometric function that is so defined that $\tilde{f} = 0$ on the surface edge, and $\tilde{f} > 0$ on the interior of the surface. Let $\hat{\nu} = \vec{\nabla}\tilde{f}$ denote the unit inward geodesic normal that lies in the plane of the surface. Let $\vec{x} = [x_1, x_2, x_3]^T$ denote the position of an observer, and by $\vec{y} = [y_1, y_2, 0]^T$ the position of a source point on the plate's surface. The unsteady perturbation pressure $p(\vec{y}, \tau)$ on the surface gives rise to sound that radiates along $\vec{r} = \vec{x} - \vec{y}$ to the observer. This sound is described by $p'(\vec{x}, t)$, the perturbation pressure that arrives at the point (x_1, x_2, x_3) at time t.

The derivation of Formulation 1B can be found in Ref. 10. However, for derivation purposes, both $\vec{x}$ and $\vec{y}$ frames of reference are considered fixed relative to the medium at rest. The resulting formulation contains a time derivative $\dot{p}$ that is evaluated relative to an observer that is fixed with respect to the medium at rest, e.g., as measured by a transducer just above the surface that remains stationary as the surface passes by it. This quantity $\dot{p}$ can be related to $\partial p/\partial\tau$, the time derivative of pressure in the reference frame of the moving surface, e.g., as measured by a transducer attached to the surface. This relation is

$$\dot{p} = \frac{\partial p}{\partial \tau} - V\,\frac{\partial p}{\partial s}$$

where $\partial p/\partial s$ is the gradient of p in the direction of $\vec{V}$, and V is the local magnitude of $\vec{V}$. Here, s is in the direction of the velocity $\vec{V}$ of the surface in the reference frame fixed to the undisturbed medium. The final expression for the sound radiated to the observer is

$$\begin{aligned} 4\pi p'(\vec{x},t) &= \int_{\tilde{f}>0} \left[\frac{(\,\partial p/\partial\tau - V\,\partial p/\partial s\,)\,\cos\theta}{c_0\,r\,(\,1-M_r\,)}\right]_{\text{ret}} dS \\ &+ \int_{\tilde{f}>0} \left[\frac{p\,\cos\theta}{r^2\,(\,1-M_r\,)}\right]_{\text{ret}} dS \qquad (1) \\ &- \int_{\tilde{f}=0} \left[\frac{M_\nu\,p\,\cos\theta}{r\,(\,1-M_r\,)}\right]_{\text{ret}} d\ell\,, \end{aligned}$$

where c_0 is the ambient sound speed, r is the magnitude of the radiation direction vector $\vec{r}$ from a point on the surface to the observer, M_r is the Mach number in the direction of $\vec{r}$, M_ν is the Mach number in the direction of the inward-facing geodesic normal $\hat{\nu}$, and θ is the angle subtended by the surface normal and the radiation vector $\vec{r}$ (See Fig. 1.). The subscript "ret" denotes evaluation at retarded time $\tau = t - r/c_0$. This is the source time at which a surface pressure fluctuation at the point $(y_1, y_2, 0)$ made its contribution to the signal detected by the observer at time t. Note that $\vec{y}, \vec{r}$, and θ are pictured in observer time in Fig. 1.

For a far field observer in a low Mach number flow, the first integral in Eq. (1) dominates the acoustic signal.

This is because the second integral in Eq. (1) is proportional to $1/r^2$ and the third integral is proportional to M. Perhaps most significant in regard to the form of Eq. (1) is that it is valid, as is, for rotating surfaces. Its predecessor, Formulation 1A,[9] is significantly more complicated in its rotational form, and cannot be approximated by only one surface integral in the far field for low Mach number flows, as can the present formulation. Such a significant simplification for far field calculations makes Formulation 1B more suitable for statistical analysis of broadband noise for rotating surfaces. A statistical formulation based on Eq. (1) was derived in Ref. 10.

3. Model Problem - Trailing Edge Tone

Any noise prediction made with Eq. (1) will be only as good as the input surface pressure $p(\vec{y},\tau)$. The current thinking is that such time-dependent pressure data would result from experimental measurement or a computational fluid dynamics (CFD) calculation. However, in this section, a simplified analytic expression is used for $p(\vec{y},t)$ to serve as a model problem. A result from thin airfoil theory[4] will be used to describe the unsteady surface pressure that is produced by the passage of a single frequency disturbance past the trailing edge of a slender airfoil. This simple surface pressure formulation will be extended to a broadband source model in the following section.

3.1 Surface Pressure from Thin Airfoil Theory

The airfoil for this model problem is a rectangular flat plate in the plane $x_3 = 0$, undergoing a uniform rectilinear motion, as in Fig. 2. The velocity vector $\vec{V} = [-U, 0, 0]^T$, where U is a constant subsonic speed. The plate's surface and its boundary, $\tilde{f} \geq 0$, are defined by the rectangle $\{ -C \leq x_1 \leq 0 \} \times \{ -b \leq x_2 \leq b \}$, with the trailing edge at $x_1 = 0$. An unsteady pressure distribution is assumed on this surface, and is analytically prescribed from thin airfoil theory, as discussed below.

Amiet[4] has proposed a formulation to model the response of an airfoil to the passage of a pressure disturbance over its trailing edge. This formulation, formally derived in Ref. 12, is based on the theory of a thin airfoil of infinite span and models the moving disturbance as stationary in the variable $x_1 - U_c t$, where U_c is the convection speed of the disturbance. The induced pressure jump on the airfoil surface can be written

$$\Delta P(x_1,t) = 2\,P_0\,g(x_1,k_c)\,e^{-ik_c(x_1-U_c t)} \qquad (2a)$$

where $k_c = \omega/U_c$ is the streamwise convective wave number, and P_0 is the amplitude of the disturbance. The factor of two in Eq. (2a) indicates that the pressure is assumed to be antisymmetric between the upper and lower surfaces, and this expression thereby accounts for the pressure on both sides of the airfoil, i.e., the pressure jump. Note that Eq. (2a) differs from the general form for the pressure jump in Ref. 10 because the explicit term $e^{-ik_c x_1}$ in Eq. (2a) was incorporated into the transfer function g in Ref. 10. The formulation in Eq. (2a) is used here for consistency with the TE noise research of Schlinker and Amiet.[16]

The transfer function $g(x_1,k_c)$ is

$$g(x_1,k_c) = -1 + (1+i)E^*[-x_1(\,k_c + \mu(1+M))] \quad (2b)$$

where $\mu = M\omega/\beta^2 U$, $\beta = \sqrt{1-M^2}$, and the function E^* is given by

$$E^*(\xi) = \int_0^\xi \frac{e^{-iu}}{(\,2\pi u\,)^{\frac{1}{2}}}\,du \;\equiv\; \mathcal{C}(\xi) - i\mathcal{S}(\xi) \qquad (2c)$$

The quantities $\mathcal{C}(\xi)$ and $\mathcal{S}(\xi)$ are the Fresnel cosine and sine integrals, and will be evaluated numerically by the formulas derived by Boersma.[18] The final representation for the unsteady surface pressure $p(y_1,\tau)$, assumed to be a real quantity, is

$$p(y_1,\tau) = \Re\{-\Delta P(y_1,\tau)\} \qquad (2d)$$

The pressure jump is negative in Eq. (2d) because the acoustic formulation in Eq. (1) is derived from a form of the Ffowcs Williams-Hawkings equation in which the unit surface normal $\hat{e}_3$ is assumed to point into the fluid, i.e., in the positive x_3 direction on the upper surface, and in the negative x_3 direction on the lower surface. Therefore, using the same positive surface normal on both sides of the airfoil, the sum of the pressure on both sides is $p = P_{\text{upper}} - P_{\text{lower}}$, and this expression is the negative of the conventional notion of a pressure jump.

Note that the transfer function in Eq. (2b) represents the effect of the induced surface pressure only, and neglects the effect of the incident pressure. The neglect of the incident pressure field effect is not of concern here, as this model problem is presented for illustrative purposes only. After the initial derivation of this induced pressure formulation,[4,12] Amiet later altered the formulation to include the effect of the incident pressure field.[5] The effects of both induced and incident surface pressure will be employed in the broadband formulation in Section 4.

3.2 Directivity Calculation

Using Eqs. (2a)–(2d) as the input surface pressure in Eq. (1), the directivity of a single frequency source is now examined. The flat plate has a chord length $C = 0.5$ meter, and a span $2\,b = 2.0$ meters. The flow speed U is determined by a free stream Mach number $M = 0.2$, with $c_0 = 343$ m/s. The disturbance amplitude P_0 is taken as one percent of the dynamic head $q_0 = \rho_0 U^2/2$, with $\rho_0 = 1.23$ kg-m/s^2, and the convection speed is taken to be $U_c = 0.8\,U$. The initial surface pressure $p(x_1,0)$, $-C \leq x_1 \leq 0$, is shown in Fig. 3. This pressure profile represents the surface pressure over the entire span at observer time $t = 0$. Note, again, that the formulation in Eqs. (2a)–(2d) represents the induced surface pressure only.

The radiated noise $p'(\vec{x},t)$ is calculated at 360 equally spaced locations on a circular arc in the plane $x_2 = 0$. The radius of this arc emanates from the mid-span location on the trailing edge, as shown in Fig. 4. The arc trajectory (r,ψ) is determined by $r = 2$ meters and $0 \leq \psi \leq 2\pi$. The surface discretization is a uniform grid of 100×400 surface elements. The directivity is determined by the peak pressure amplitude calculated at each

position, during one period $T = 1/f$ for a frequency of 2.5 kHz, with 128 timesteps in a period. Fig. 5 shows the results, in polar form, where the notation $||p'||$ is interpreted as

$$||p'|| = \max_{0<t<T} |p'(\vec{x}, t)|$$

The upstream directivity of the major lobes is consistent with the research of previous authors, e.g., Singer, et al [8].

3.3 Velocity Scaling Law

Attention is now turned to the way in which the intensity of the far field noise, as predicted by Eq. (1), will scale as a function of velocity, when the surface pressure is described by Eqs. (2a)–(2d). A scaling law will be determined under the assumption that the acoustic source is noncompact, i.e., $\lambda \ll C$. Furthermore, the observer is assumed to be in the acoustic and geometric far field, i.e., $r \gg \lambda$ and $r \gg C$, respectivey.

Because scaling laws are typically determined for low Mach number flows,[3,19] the Mach number range of interest is $0.01 \leq M \leq 0.2$. The surface pressure amplitude P_0 is one percent of the dynamic head. The plate's physical dimensions are the same as in the above directivity problem. The observer is chosen at a distance of 10 meters, directly above the trailing edge, i.e., $\vec{x} = [\,0, 0, 10\,]^T$ in meters. The calculations are performed on a 100×400 uniform surface grid.

The surface pressure in Eqs. (2a)–(2d), with a frequency of 2.5 kHz, is used as input to equation to Eq. (1) to predict the far field sound $p'(\vec{x}, t)$ to the observer. A separate calculation is run for each of 50 equally spaced Mach numbers between 0.01 and 0.2. Each calculation is performed for one period with 128 timesteps. The average intensity $I(\vec{x})$ of the acoustic signal at the observer $\vec{x}$, assuming spherical spreading, is then calculated by

$$I(\vec{x}) = \frac{1}{T} \int_0^T \frac{[\,p'(\vec{x}, t)\,]^2\, dt}{\rho_0\, c_0}$$

The average acoustic intensities for this test case, as a function of Mach number, are represented as circles in Fig. 6. The slope of these results on a log-log plot can be visually determined by observing their proximity to the dotted line whose slope is exactly five. This U^5 proportionality is consistent with the result of Ffowcs Williams and Hall,[3] as expected from the idealized conditions placed upon the calculations.

4. Broadband Predictions

The analytic surface pressure in the previous section is extended to model a broadband trailing edge source on a slender airfoil at zero angle of attack. Following the approach of Schlinker and Amiet,[16] the surface pressure correlations required as input are evaluated by flat plate theory and by experimental measurements. This broadband surface pressure is used as input to Formulation 1B to predict far field radiation in the time domain. The results are Fourier analyzed and compared with experimental TE noise spectra.[17]

4.1 Experiment Description

The experiment that is modeled in this section is reported by Brooks and Hodgson.[17] A NACA 0012 airfoil is placed between two plates at zero angle of attack in the test section of an open jet wind tunnel. A schematic of this experimental setup is shown in Fig. 7. Noise propagates from the test section into an anechoic chamber that is instrumented with microphones.

The airfoil has a chord length of 0.6096 m and a span of 0.46 m. The tunnel speeds of interest here are 38.6 m/s and 69.5 m/s. The chord-based Reynolds numbers are 1.57 million and 2.82 million, respectively. Boundary layer tripping was applied at 15 percent chord downstream of the leading edge to ensure a spanwise uniform transition location and a fully developed turbulent boundary layer at the trailing edge.

For radiated noise measurements, eight microphones are located in the plane perpendicular to the airfoil midspan. The presence of extraneous noise sources precludes direct mearurement of TE noise by a single microphone. Therefore, to evaluate the TE noise, a cross-spectral analysis of pairs of microphones was employed in a manner consistent with the coherent output power method.[20,21] The microphone pictured in Fig. 7 represents the location for which the current predictions are made, at a distance of 1.22 m directly above the airfoil trailing edge. Note that a shear layer forms downstream of the nozzle lip, between the airfoil and the microphone. Although both the directivity and the amplitude of the TE noise are affected by refraction through this shear layer, the corrections for the microphone at this location are small enough to ignore (see Ref. 17).

4.2 Broadband Analysis

For prediction purposes, the airfoil is modeled as a flat plate in order to evaluate the unsteady surface pressure with a broadband extension of the analytic formulation in Section 3. The airfoil geometry is oriented with respect to the coordinate axes as in Fig. 2, with $\{\,-C \leq x_1 \leq 0\,\} \times \{\,-b \leq x_2 \leq b\,\}$, where $C = 0.6096$ m and $2b = 0.46$ m.

The surface pressure arises from boundary layer turbulence that is assumed to convect in a frozen pattern along the airfoil surface towards the trailing edge. Unlike the single frequency source in Section 3, the broadband nature of the surface pressure in the present case requires consideration of both chordwise and spanwise wave numbers, k_1 and k_2, respectively. Each Fourier component of this broadband surface pressure jump is associated with a wave number pair (k_1, k_2) and can be written

$$\Delta P(k_1, k_2;\, x_1, x_2, t) = \tag{3}$$

$$2\tilde{P}(k_1, k_2)\, g(x_1, k_1, k_2)\, e^{-i[k_1(x_1 - U_c t) + k_2 x_2]}$$

where $\tilde{P}(k_1, k_2)$ is the amplitude of the pressure jump associated with the wave number pair (k_1, k_2). Because of

the assumed convective nature of the turbulence, the notation for the chordwise wave number k_1 will be replaced by k_c to emphasize its dependence on the convection speed U_c and to avoid confusion with the conventional notion of $k_1 = \omega/U$. In an exact sense, there are infinitely many combinations of frequency and convection speed whose ratio ω/U_c yields a given value of k_c. However, it is assumed here that the acoustically relevant structures in the turbulent boundary layer are frozen with respect to a single convection speed that is taken as $U_c = 0.8\,U$.

The complete broadband spectrum for the surface pressure jump $\Delta P(x_1, x_2, t)$ is obtained by summing all Fourier components in Eq. (3):

$$\Delta P(x_1, x_2, t) = \tag{4}$$
$$2\int_{-\infty}^{\infty}\int_{-\infty}^{\infty} \tilde{P}(k_c, k_2)\, g(x_1, k_c, k_2)\, e^{-i\,[k_c(x_1 - U_c t) + k_2 x_2]}\, dk_c\, dk_2$$

A straightforward approach for predicting the desired broadband far field measurements is to use the real part of Eq. (4) as input to Formulation 1B. This approach requires knowledge of a two-component surface pressure spectrum and a dual wave number transfer function $g(x_1, k_c, k_2)$. However, because one of the objectives of the current work is to reproduce the results of Schlinker and Amiet[16] from a time domain perspective, an approach similar to that taken in Ref. 16 will be used to model the surface pressure.

The analysis for the general formulation in Ref. 16 comes from previous work[22] in which Amiet argues that, within certain limitations, integration over all spanwise wave numbers is not required. His conclusion, derived mathematically in the frequency domain, is that only one spanwise wave number contributes to the sound detected by an observer in a given location. In particular, Amiet focuses on an observer in a spanwise symmetric location, for which only the zero spanwise wave number needs to be considered. This result is argued to be exact in the limit of infinite span and a good approximation for an airfoil of finite span that responds to a high frequency disturbance. Although Amiet's analysis was initially presented to derive an acoustic formulation for incidenct turbulence noise, the result pertaining to spanwise wave numbers is sufficiently general to apply to the present trailing edge problem.

The derivation of Amiet's analytical result can be generally described as follows. First, Eq. (4) is transformed into Fourier space. Then, a two-point cross-correlation function is formed and related to the far field power spectrum through Kirchhoff's formula[23] and Curle's result.[19] In order to follow a similar line of reasoning in the time domain, Eq. (4) itself must be related to the far field acoustic pressure through Formulation 1B. In the case of a distant observer directly overhead of a finite-span airfoil, the terms r, M_r, and θ in Eq. (1) are weak functions of y_1 and y_2 on the airfoil surface, and therefore will be considered constants. Furthermore, for the observer position considered here, the differences in retarded time, as a function of airfoil surface location, can be neglected. These assumptions are consistent with the acoustic model employed by Amiet.[22] For the present problem, including the above assumptions, Eq. (1) is approximated by

$$4\pi p'(\vec{x}, t) \approx \tag{5}$$
$$\frac{\cos\bar{\theta}}{c_0 \bar{r}(1-\bar{M}_r)} \int_0^C \int_{-b}^{b} \left[\frac{\partial}{\partial \bar{\tau}} p(\vec{y}, \bar{\tau}) + U \frac{\partial}{\partial y_1} p(\vec{y}, \bar{\tau}) \right] d\vec{y}$$

where the over-bars on $\bar{\theta}, \bar{r}$, and $\bar{M}_r$ denote mean values over the airfoil surface, and therefore the retarded time $\bar{\tau} = t - \bar{r}/c_0$ is constant for fixed t. Recall that only the first integral in Eq. (1) is significant under the present assumptions of a far field observer in a low Mach number flow.

Before the surface pressure $p(\vec{y}, \bar{\tau})$ is specified, Eq. (5) is further simplified. For convenience, the terms $\bar{\theta}$ and $\bar{M}_r$ will be neglected, as they are small ($\bar{M}_r \approx 0$ and $\cos\bar{\theta} \approx 1$) for a distant observer directly above the airfoil. With these additional simplifications, if $-\Delta P$ in Eq. (4) is substituted for $p(\vec{y}, \bar{\tau})$ in Eq. (5), the far field acoustic pressure can be approximated in the form

$$4\pi p'(\vec{x}, t) \approx \frac{2}{c_0\,\bar{r}} \int_0^C \int_{-b}^{b} \int_{-\infty}^{\infty} \int_{-\infty}^{\infty} \mathcal{F}(y_1, k_c, k_2)$$
$$\times \quad e^{-i\,[k_c(y_1 - U_c\bar{\tau}) + k_2 y_2]}\, dk_2\, dk_c\, dy_2\, dy_1 \tag{6a}$$

where

$$\mathcal{F}(y_1, k_c, k_2) = \tag{6b}$$
$$-\tilde{P}(k_c, k_2) \left[ik_c(U_c - U) g(y_1, k_c, k_2) + U \frac{\partial}{\partial y_1} g(y_1, k_c, k_2) \right]$$

Sufficient conditions[24] on ΔP and its derivatives have been assumed for the commutation of integration and differentiation in Eqs. (6a) and 6(b). The y_2 integration in Eq. (6a) can now be explicitly evaluated, yielding

$$4\pi p'(\vec{x}, t) \approx \frac{2}{c_0\,\bar{r}} \int_0^C \int_{-\infty}^{\infty} \int_{-\infty}^{\infty} \frac{2\,\sin(k_2 b)}{k_2}\, \mathcal{F}(y_1, k_c, k_2)$$
$$\times \quad e^{-i\,k_c(y_1 - U_c\bar{\tau})}\, dk_2\, dk_c\, dy_1 \tag{7}$$

Integrating with respect to k_2, the term $\sin(k_2 b)/k_2$ acts like a Dirac delta function when integrating over an unbounded domain, and the result is

$$4\pi p'(\vec{x}, t) \approx \frac{2}{c_0\,\bar{r}} \int_0^C \int_{-\infty}^{\infty} 2\pi \mathcal{F}(y_1, k_c, 0)\, e^{-ik_c(y_1 - U_c\bar{\tau})}\, dk_c\, dy_1 \tag{8}$$

Eq. (8) indicates that only the zero spanwise wave number contributes to the noise detected by the far field observer. Eqs. (7) and (8) are time domain analogies to Eqs. (15) and (17) in Ref. 22. Furthermore, Eq. (8) suggests that the acoustic source $p(\vec{y}, \tau)$ in Eq. (1) can be evaluated as the real part of a simplified pressure jump:

$$\Delta P(x_1, t) \;=\; 2\pi \int_{-\infty}^{\infty} \tilde{P}(k_c, 0)\, g(x_1, k_c, 0)\, e^{-ik_c(x_1 - U_c t)}\, dk_c$$
$$p(\vec{y}, \tau) \;=\; \Re\{-\Delta P(y_1, \tau)\} \tag{9}$$

Note that, when performing the actual calculation, the y_2 integration will be explicitly performed when Eq. (9) is input to Eq. (6). Only the k_2 integration will be neglected. Furthermore, the evaluation of the surface pressure terms at retarded time $\tau = t - r/c_0$ will be executed in an exact fashion, as prescribed by Eq. (1). All three integrals in Eq. (1) will be evaluated for the predictions that follow, although the first integral is expected to dominate the signal.

The evaluation of the surface pressure in Eq. (9) is accomplished by first recognizing the turbulent fluctuations as a stochastic process. This process can be approximated by a truncated series whose limit exhibits the required relationship between the autocorrelation and the power spectrum of that process (e.g., Ref. 25). This relationship is achieved by evaluating the pressure amplitudes $\tilde{P}(k_c, k_2)$ as a function of Φ_{PP}, the power spectral density (PSD) of the surface pressure. To this end, the infinite wave number domain, $-\infty < k_c < \infty$, in Eq. (9) is integrally discretized and truncated such that $k_{c,-N} < k_{c,n} < k_{c,N}$. The largest convective wave number $k_{c,N}$ represents an "upper cutoff" wave number, beyond which the surface pressure amplitude $\tilde{P}(k_c, 0)$ is considered negligible or is out of range of experimental measurement. The unsteady surface pressure jump in Eq. (9) is then approximated by

$$\Delta P(x_1,t) \approx 2\pi \sum_{n=-N}^{N} A_{n,0} e^{i\phi_n} g(x_1, k_{c,n}, 0) e^{-i\,k_{c,n}\,(x_1 - U_c t)} \tag{10a}$$

$$k_{c,n} = n\,\Delta k_c\,, \qquad n = 0, \pm 1, \pm 2, \ldots, \pm N$$

$$\Delta k_c = k_{c,N}/N$$

The discrete surface pressure amplitudes $\{A_{n,0}\}$ are evaluated by

$$A_{n,0} = [\,\Phi_{PP}(k_{c,n}, 0)\,\Delta k_c\,]^{\frac{1}{2}} \tag{10b}$$

where $\Phi_{PP}(k_c, k_2)$ is the two-component PSD of the surface pressure. Amiet[16] argues that the required single wave number spectrum $\Phi_{PP}(k_c, 0)$ can be evaluated by

$$\Phi_{PP}(k_c, 0) = \frac{U_c}{\pi}\ \ell_{x_2}(\omega)\, S_{qq}(\omega, 0) \tag{10c}$$

where $\ell_{x_2}(\omega)$ is the spanwise correlation length and $S_{qq}(\omega, \Delta x_2)$ is the spanwise surface pressure correlation function.

The phase angles $\{\phi_n\}$ are independent random variables uniformly distributed on $[\,0,\, 2\pi]$. The transfer function in Eq. (2b) can be used for $g(x_1, k_{c,n}, 0)$ with the following modification. As previously noted, Eqs. (2a) and (2b) represent the induced pressure jump. Amiet[5] has suggested that the incident pressure, i.e., that which results from turblent eddies that contact the trailing edge, can be accounted for by the addition of an exponential convergence factor of the form $e^{\epsilon k_c x_1}$, where ϵ is a positive parameter. For $-C \le x_1 \le 0$, this additional term will be significantly larger than zero only in the immediate vicinity of the trailing edge, provided that $\epsilon k_c C$ is large. Therefore, to include the effect of the incident pressure, the transfer function to be used in Eq. (10a) is the two-component function $g(x_1, k_c, k_2)$ in Ref. 16, with $k_2 = 0$.

$$g(x_1, k_c, 0) = e^{\epsilon k_c x_1} - 1 + (1+i) E^*[-x_1(k_c + \mu(1+M))] \tag{10d}$$

where E^* is the same complex combination of Fresnel integrals as in Eq. (2c). Amiet[5] was able to avoid the direct use of the parameter ϵ because of the manner in which the transfer function in Eq. (10d) was used in his analysis. Amiet used the transfer function to define an unsteady lift response function that involved the chordwise integration of the transfer function with other terms. The result of this integration yields an expression that, upon clever manipulation of limits, does not contain ϵ but still provides an additional term to the lift response function that accounts for the incident pressure. In the present case, the transfer function in Eq. (10d) must be explicitly used and therefore a value for ϵ must be specified. This value $\epsilon = 1.5$ is chosen for reasons that are discussed in the following subsection.

To illustrate the effect of including this incident pressure term in the surface pressure formulation, Fig. 8 shows the same single frequency surface pressure case in Section 3, with and without the the incident pressure term. Clearly, the incident pressure term has a significant effect only near the trailing edge, as expected. However, for a given frequency, differing values of ϵ will result in differing amounts of upstream chordlength to be so affected. Note that the addition of this term causes the pressure jump to vanish at the trailing edge for all time, i.e., the Kutta condition is satisfied. Note also the increase in spatial oscillation that is caused near the trailing edge when the effect of this incident pressure term is included.

Eqs. (10a)–(10d) represent the the complex-valued broadband surface pressure formulation to be used for the present TE noise predictions. The final representation for the unsteady broadband pressure on the airfoil surface is then given by the real part of $-\Delta P$ in Eq. (10a). Using symmetry arguments and algebraic manipulation, the indicial bounds for the surface pressure's spectral representation are altered so that the domain includes only positive wave numbers. As input to Eq. (1), the resulting real-valued surface pressure can be written

$$p(y_1,\tau) = -4\pi \sum_{n=1}^{N} A_{n,0}\{\, B_n \cos[k_{c,n}(y_1 - U_c\tau) + \phi_n] + D_n \sin[k_{c,n}(y_1 - U_c\tau) + \phi_n]\,\} \tag{11a}$$

where

$$A_{n,0} = \left[\frac{U_c}{\pi}\,\ell_2(\omega_n)\, S_{qq}(\omega_n, 0)\,\Delta k_c\right]^{\frac{1}{2}} \tag{11b}$$

$$B_n = e^{\epsilon k_{c,n} y_1} - 1 + \mathcal{C}(\xi_n) + \mathcal{S}(\xi_n) \tag{11c}$$

$$D_n = \mathcal{C}(\xi_n) - \mathcal{S}(\xi_n) \tag{11d}$$

$$\xi_n = -y_1[k_{c,n} + \mu_n(1+M)] \tag{11e}$$

and $\mathcal{C}(\xi_n)$ and $\mathcal{S}(\xi_n)$ are the Fresnel cosine and sine integrals in Eq. (2c). Specific evaluations for the correlation

lengths ℓ_2 and surface pressure correlations S_{qq} will be discussed in the following section.

4.3 Time Domain Predictions

The lower and upper frequency bounds for both calculations are 25 Hz and 10 kHz, respectively. Therefore, $f = 25$ Hz also serves as the fundamental frequency and the numerical bandwidth Δf. Each calculation is performed for one period of the lowest frequency, $T = 0.04$ s. The numerical solution is sampled at the Nyquist frequency, i.e., $\Delta t = T/2N$. The calculation is performed on a 500×100 surface grid with grid-point clustering near the trailing edge, as shown in Fig. 9. This trailing edge clustering allows for better resolution to account for the effect of the incident pressure term in Eq. (10d), as previously shown in Fig. 8. As in the constant frequency case, because the surface pressure in Eqs. (11a)–(11e) is cast in only one spatial variable y_1, and the observer location is symmetric relative to the airfoil span, the acoustic predictions are found to be relatively insensitive to the discretization in y_2, and the primary concern for grid resolution is in the streamwise direction. With 500 points in the streamwise direction and clustering near the trailing edge, a sufficient resolution of at least 10 points per wavelength was obtained for the entire length of the chord. This conclusion was reached by inspection of surface pressure profiles for the highest frequency of 10 kHz.

The coordinate system for the calculation is such that the x_2-axis coincides with the center span line, so that the microphone position is in the plane $x_2 = 0$. The experimental microphone position for which comparisons are made is at a distance of 1.22 m from the model, and at an angle of 90 degrees relative to the chord and directly above the trailing edge. The measured observer position for the prediction is, then, $\vec{x} = [\,0,\ 0,\ 1.22\,]^T$ in meters.

The baseline prediction case under consideration is for a tunnel speed of $U = 69.5$ m/s. This flow condition, the above observer location, and airfoil geometry are incorporated into an acoustic prediction using Eq. (1) with the surface pressure defined by Eqs. (11a)–(11e). Following the example of Schlinker and Amiet,[16] a first-cut prediction is performed using flat plate theory to evaluate the surface pressure correlations $S_{qq}(\omega, 0)$ and spanwise corelation lengths $\ell_2(\omega)$ in Eq. (11b). The authors used empirical formulations for these quantities that they derived from previous analysis and boundary layer measurements of Corcos[26] and Willmarth and Roos.[27] The surface pressure correlations are approximated by

$$S_{qq}(\omega, 0) \approx q_0^2 \, \frac{\delta^*}{U} \, \frac{2 \times 10^{-5}}{1 + \tilde{\omega} + 0.217\,\tilde{\omega}^2 + 0.00562\,\tilde{\omega}^4} \tag{12a}$$

where $q_0 = \rho_0 U^2/2$, δ^* is the trailing edge displacement thickness, and $\tilde{\omega} = \omega \delta^*/U$. The displacement thickness is also taken from a flat plate approximation for turbulent boundary layer thickness δ on a flat plate, based on the chord Reynolds number Re_C, i.e.,

$$\frac{\delta}{C} \approx \frac{0.37}{(Re_C)^{\frac{1}{5}}} \approx 8\,\frac{\delta^*}{C} \tag{12b}$$

For the experiment of Brooks and Hodgson,[17] Schlinker and Amiet[16] used Eq. (12b) to compute the boundary layer thickness δ and accounted for boundary layer tripping by taking the 15 percent chord station as the initial point of the calculation. Surface curvature was also accounted for in the downstream distance used in the calculation. The ratio δ/C used by Schlinker and Amiet for this experiment was reported as 0.0166 for $U =$ 69.5 m/s and 0.0187 for $U = 38.6$ m/s. The displacement thickness was then taken as 1/8 of the boundary layer thickness. The expression that Schlinker and Amiet[16] suggest for the spanwise correlation length is

$$\ell_2(\omega) \approx \frac{2.1\,U_c}{\omega} \tag{12c}$$

Fig. 10 shows the far field signal $p'(\vec{x}, t)$ that is predicted by Formulation 1B at the experimental microphone location, for a tunnel speed of 69.5 m/s. The surface pressure is modeled with Eqs. (11a)–(11e) and (12a)–(12c). The time signal $p'(\vec{x}, t)$ is Fourier analyzed to determine a discrete set of spectral amplitudes $\{P_n\}_{n=1}^N$. The far field sound pressure level (SPL) spectrum is calculated by

$$\mathrm{SPL}(f_n) = 20\,\log\left[\,\frac{P_n}{P_{\mathrm{ref}}}\,\right] \quad , \qquad n = 1, 2, \ldots, N \tag{13}$$

where the reference pressure is $P_{\mathrm{ref}} = 20\,\mu$Pa. The SPLs are converted to a 1.0 Hz bandwidth by reducing the values in Eq. (13) by $10\,\log(\Delta f)$.

The resulting narrowband SPLs are compared with the prediction of Schlinker and Amiet[16] in Fig. 11. Also on this plot are the narrowband SPLs that were experimentally measured by Brooks and Hodgson.[17] The predicted results of Schlinker and Amiet and the measurements of Brooks and Hodgson were obtained by digitizing the appropriate plots in Figure 34 of Ref. 16. Various values of the paramenter ϵ in Eq. (10d) were assessed in this comparison stage of the research. With an arbitrary parameter in the formulation, the value $\epsilon = 1.5$ was chosen for its agreement with the flat plate correlation results of Schlinker and Amiet.[16] This value of ϵ is held fixed at 1.5 for all remaining calculations.

Clearly, Fig. 11 shows that significant error exists between the predictions and the measurements when flat plate formulations are used for the required surface pressure correlations. Fig. 12 sheds light on this error with a comparison of the flat plate formula in Eq. (12a) and the measured surface pressure correlations of Yu and Joshi.[28] The notation $\bar{S}_{qq}$ denotes that the surface pressure correlations are normalized by $q_0^2\,\delta^*/U$. The measured data in Fig. 12 were obtained by digitizing the "average" plot in Figure 35(a) of Ref. 16. The normalized flat plate surface pressure correlations are significantly lower than the measured data, by as much as 7 dB. The reason that the flat plate approximation is so much in error is only in small part because of the the lack of pressure gradient. The most significant error made in the approximation in Eq. (12a) is the lack of a trailing edge; this empirical formulation is based on experimental measurement and analysis in which the flat plate is assumed to be infinite. Clearly, surface pressure correlations that are based

on flat plate theory are inappropriate for predicting TE noise in this case.

The experimental surface pressure correlations[28] in Fig. 12 will now be used in the surface pressure formulation to predict the TE noise associated with the two tunnel speeds of interest and compared with experimental measurements. The modified formula for the surface pressure correlations is

$$S_{qq}(\omega,0) \approx q_0^2 \, \frac{\delta^*}{U} \, \bar{S}_{qq}(\omega,0) \tag{14}$$

where $\bar{S}_{qq}(\omega,0)$ denotes the normalized measured data in Fig. 12. The tabulated data obtained from digitizing this information from Ref. 16 is stored in a file that is accessed and interpolated to obtain $\bar{S}_{qq}(\omega,0)$ for any frequency. Having altered the surface pressure correlation function by experimental data, the evaluation of the spanwise correlation length is now brought into question. However, it was concluded by Brooks and Hodgson[17] that the function $\ell_2(\omega)$ for a flat plate and a thin airfoil are identical under suitable normalization. Therefore, the use of Eq. (12c) for $\ell_2(\omega)$ will be retained for the remaining calculations.

The predicted and measured far field SPLs for the two tunnel speeds are shown in Fig. 13. The experimental data in Fig. 13 were obtained by digitizing the measurements plotted in Figure 34 of Reference 16. The agreement with the measured data is significantly improved when the calculation includes surface pressure correlations that account for the trailing edge of an airfoil. In fact, it was concluded by Schlinker and Amiet[16] that airfoil surface pressure correlations were absolutely necessary for realistic TE noise predictions.

Concluding Remarks

The prediction of broadband trailing edge noise from rotating machinery and airframes is currently the subject of intense research in aeroacoustics. The physics of broadband noise generation are well understood as the result of the pioneering research of Howe,[14,29,30] Amiet and coworkers,[4,5,12,16,22] and Brooks and coworkers.[17,31] The previous work of these aeroacousticians, and many others, has clearly demonstrated that any successful broadband loading noise prediction requires an understanding of two physical processes: the character of the time-dependent surface pressure that provides the acoustic source, and the manner in which that source gives rise to an acoustic signal.

Obtaining the fluctuating surface pressure distribution analytically, numerically, or experimentally is itself a difficult problem. For this reason, past researchers have most often resorted to modeling the surface pressure, using guidance from experiments to aid in the development of these models. Today, high resolution surface pressure fluctuations can be obtained from turbulence simulations in realistic situations where the airfoil geometry and kinematics are accurately modeled. Therefore, the improvement of the acoustic radiation model becomes an important research topic. In the past, acoustic radiation models were most often developed for airfoils in uniform rectilinear motion. In addition, other restrictive assumptions, such as far field positioning of the observer, were often used to simplify the acoustic analysis.

The present work further develops a simple and general acoustic result in the time domain, based on the solution of the loading noise term of the Ffowcs Williams-Hawkings equation. This new solution, called Formulation 1B, is, to date, the simplest analytical result for the prediction of loading noise and is suitable for statistical analysis of broadband noise for a surface in general motion. The new formulation has been validated with time domain calculations that predict trailing edge noise on a NACA 0012 airfoil in a low Mach number flow. The time domain predictions are found to be in excellent agreement with the frequency domain predictions of Schlinker and Amiet[16] as well as with the experimental measurements of Brooks and Hodgson.[17] These results are, to the authors' knowledge, the first successful broadband trailing edge noise predictions in the time domain.

The authors advocate the use of time domain methods in the prediction of broadband noise. Because of the decoupling of the aerodynamics from the acoustics, the chief advantage of time domain methods is their potential for direct use of time-dependent surface pressure statistics from experiments or computer simulations.

Acknowledgements

The authors would like to express their gratitude to Dr. Roy K. Amiet, whose input from his past experience was invaluable to this research. The authors are also grateful to Dr. Meelan Choudhari of NASA Langley Research Center for several enlightening discussions on the subject of stochastic modeling.

References

1. Howe, M. S., "A Review of the Theory of Trailing Edge Noise," *Journal of Sound and Vibration*, Vol. 61, 1978, pp. 437–465.

2. Lighthill, M. J., "On Sound Generated Aerodynamically. I. General Theory," *Proceedings of the Royal Society of London*, A 211, 1952, pp. 564–587.

3. Ffowcs Williams, J. E. and Hall, L. H., "Aerodynamic Sound Generation by Turbulent Flow in the Vicinity of a Scattering Half-Plane," *Journal of Fluid Mechanics*, Vol. 40, 1970, pp. 657–670.

4. Amiet, R. K., "Noise Due to a Turbulent Flow Past a Trailing Edge," *Journal of Sound and Vibration*, Vol. 47, No. 3, 1976, pp. 387–393.

5. Amiet, R. K., "Effect of the Incident Surface Pressure Field on Noise Due to a Turbulent Flow Past a Trailing Edge," *Journal of Sound and Vibration*, Vol. 57, No. 2, 1978, pp. 305–306.

6. Goldstein, M. E., "Scattering and Distortion of the Unsteady Motion on Transversely Sheared Mean Flows," *Journal of Fluid Mechanics*, Vol. 91, No. 4, 1979, pp. 601–632.

7. Ffowcs Williams, J. E. and Hawkings, D. L., "Sound Generation by Turbulence and Surfaces in Arbitrary

Motion," *Philosophical Transactions of the Royal Society*, A 264, 1969, pp. 321–342.

8. Singer, B. A., Brentner, K. S., Lockard, D. P., and Lilley, G. M., "Simulation of Acoustic Scattering from a Trailing Edge," *Journal of sound and Vibration*, Vol. 230, No. 3, 2000, pp. 541–560.

9. Farassat, F. and Succi, G. P., "The Prediction of Helicopter Rotor Discrete Frequency Noise," *Vertica*, Vol. 7, No. 4, 1983, pp. 309–320.

10. Casper, J. and Farassat, F., " Broadband Noise Predictions Based on a New Aerocoustic Formulation," AIAA Paper No. 2002-0802.

11. Paterson, R. W., and Amiet, R. K., "Noise and Surface Pressure Response of an Airfoil to Incident Turbulence," *AIAA Journal of Aircraft*, Vol. 14, No. 8, 1977, pp. 729–736.

12. Amiet, R. K., "High Frequency Thin-Airfoil Theory for Subsonic Flow," *AIAA Journal*, Vol. 14, No. 8, 1976, pp. 1076–1082.

13. Willmarth, W. W. and Roos, F. W., "Reslution and Structure of the Wall Pressure Field Beneath a Turbulent Boundary Layer," *Journal of Fluid Mechanics*, Vol. 22, 1965, pp. 81–94.

14. Corcos, G. M., "The Structure of the Turbulent Pressure Field in Boundary Layer Flows," *Journal of Fluid Mechanics*, Vol. 18, 1964, pp. 353–378.

15. Yu, J. C. and Joshi, M. C., "On Sound Radiation from the Trailing Edge of an Isolated Airfoil in a Uniform Flow," AIAA Paper No. 79-0603, 1979.

16. Schlinker, R. H., and Amiet, R. K., "Helicopter Rotor Trailing Edge Noise," NASA Contractor Report No. 3470, 1981.

17. Brooks, T. F., and Hodgson, T. H., "Trailing Edge Noise Prediction from Measured Surface Pressures," *Journal of Sound and Vibration*, Vol. 78, No. 1, 1981, pp. 69–117.

18. Boersma, J., "Computation of Fresnel Integrals," *Mathematics of Computation*, Vol. 14, 1960, p. 380.

19. Curle, N., "The Influence of Solid Boundaries on Aerodynamic Sound," *Proceedings of the Royal Society of London*, A 231, 1954, pp. 505–514.

20. Halvorsen, W. G. and Bendat, J. S., "Noise Source Identification Using Coherent Output Power Spectra," *Journal of Sound and Vibration*, Vol. 9, 1975, pp. 15–24.

21. Piersol, A. G., "Use of Coherence and Phase Data Between Two Receivers in Evaluation of Noise Environments," *Journal of Sound and Vibration*, Vol. 56, pp. 215–228.

22. Amiet, R. K., "Acoustic Radiation from an Airfoil in a Turbulent Stream," *Journal of Sound and Vibration*, Vol. 41, 1975, pp. 407–420.

23. Lamb, H., *Hydrodynamics*, Dover Publications, New York, 6th edition, p. 501.

24. Courant, R. and John, F. *Introduction to Calculus and Analysis*, Vol. 2, Springer-Verlag, New York, 1989.

25. Shinozuka, M. and Deodatis, G., "Simulation of Stochastic Processes by Spectral Representation," *Applied Mechanics Review*, Vol. 44, No. 4, 1991, pp. 191–204.

26. Corcos, G. M., "The Structure of the Turbulent Pressure in Boundary Layer Flows," *Journal of Fluid Mechanics*, Vol. 18, 1964, pp. 353–378.

27. Willmarth, W. W. and Roos, F. W., "Resolution and Structure of the Wall Pressure Field Beneath a Turbulent Boundary Layer," *Journal of Fluid Mechanics*, Vol. 22, 1965, pp. 81–94.

28. Yu, J. C. and Joshi, M. C., "On Sound Radiation from the Trailing Edge of an Isolated Airfoil in a Uniform Flow," AIAA Paper No. 79-0603, 1979.

29. Howe, M. S., "Trailing Edge Noise at Low Mach Numbers," *Journal of Sound and Vibration*, Vol. 225, No. 2, 1999, pp. 211–238.

30. Howe, M. S., "Trailing Edge Noise at Low Mach Numbers, Part 2: Attached and Separated Flows," *Journal of Sound and Vibration*, Vol. 234, No. 5, 2000, pp. 761–775.

31. Brooks, T. F., Pope, D. S., and Marcolini, A. M., "Airfoil Self-Noise and Prediction," NASA RP-1218, July, 1989.

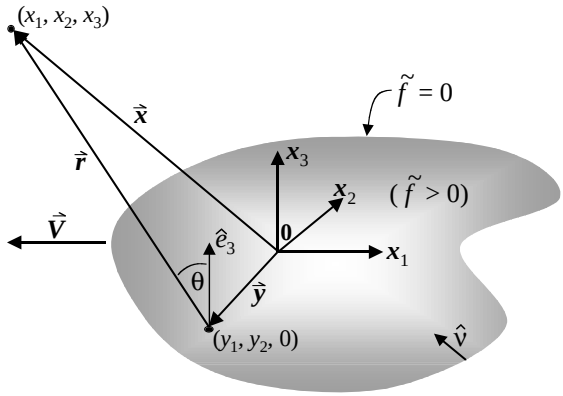

Fig. 1 Schematic for Formulation 1B (Eq. (1)).

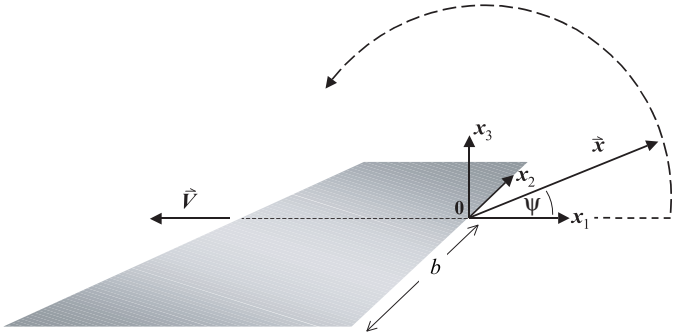

Fig. 4 Schematic for directivity calculation. Observer on circular path in plane $x_2 = 0$.

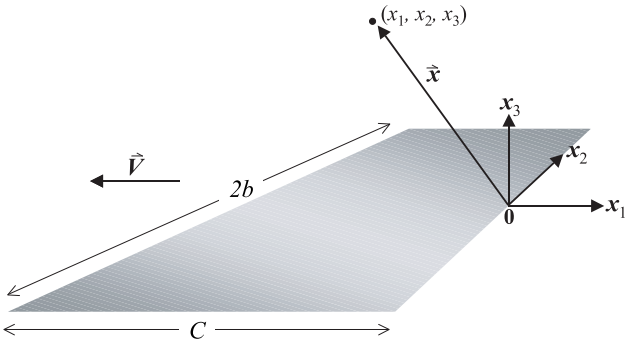

Fig. 2 Schematic for the constant-frequency trailing edge noise problem in Section 3.

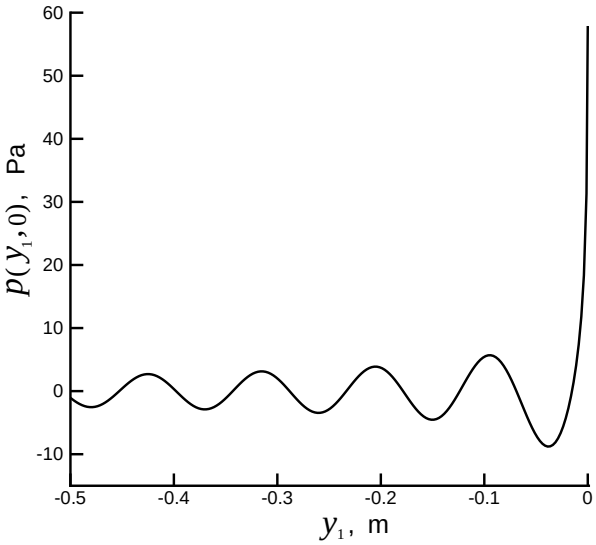

Fig. 3 Initial surface pressure profile using Eqs. (2a)–2(d).

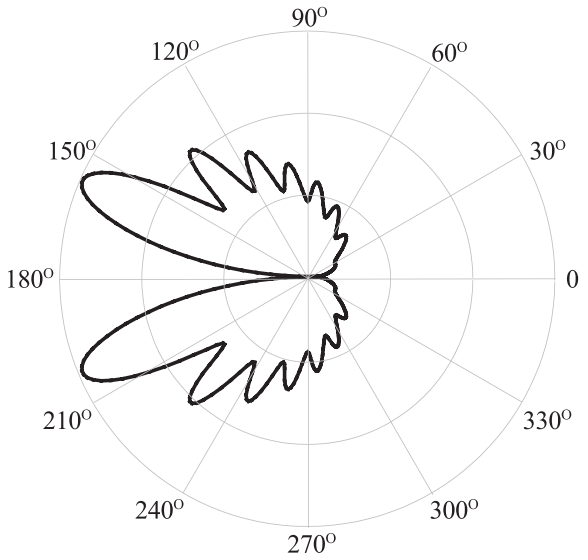

Fig. 5 Directivity for a constant frequency source of 2.5 kHz; observer distance 2 m; spacing between concentric circles on grid represents 0.25 Pa.

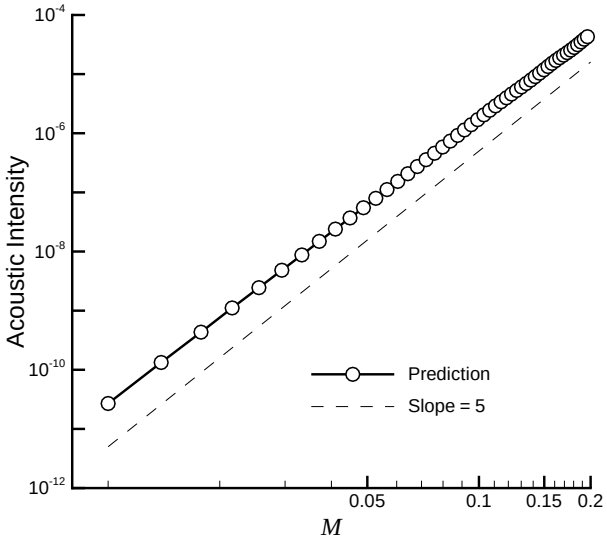

Fig. 6 Velocity scaling properties as determined by Formulation 1B and the surface pressure in Eqs. (2a)–(2d).

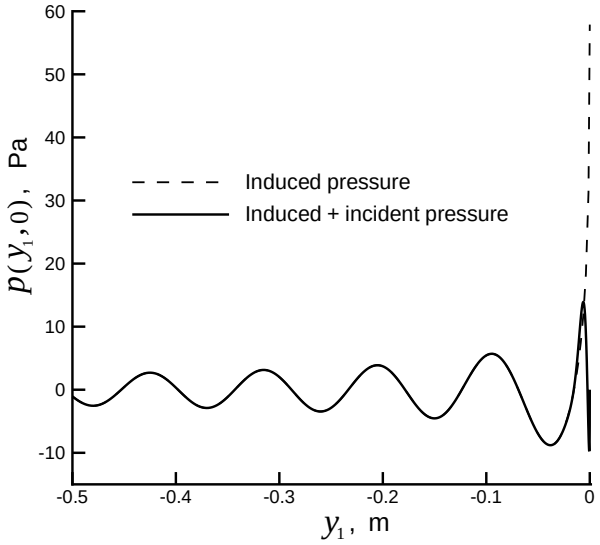

Fig. 8 Effect of incident pressure term on initial surface pressure profile using Eqs. (2a)–2(d), and modified with Eq. (10d).

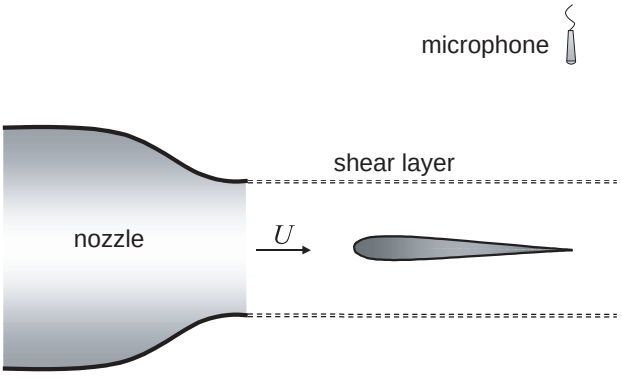

Fig. 7 Schematic for trailing edge noise experiment of Brooks and Hodgson.[17]

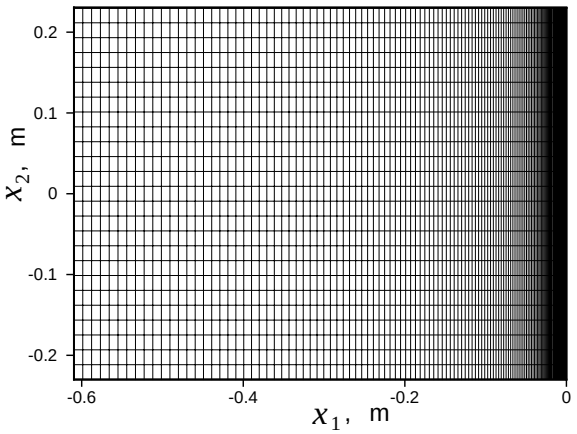

Fig. 9 Surface grid for prediction of experiment of Brooks and Hodgson,[17] every fourth point of in each direction is shown.

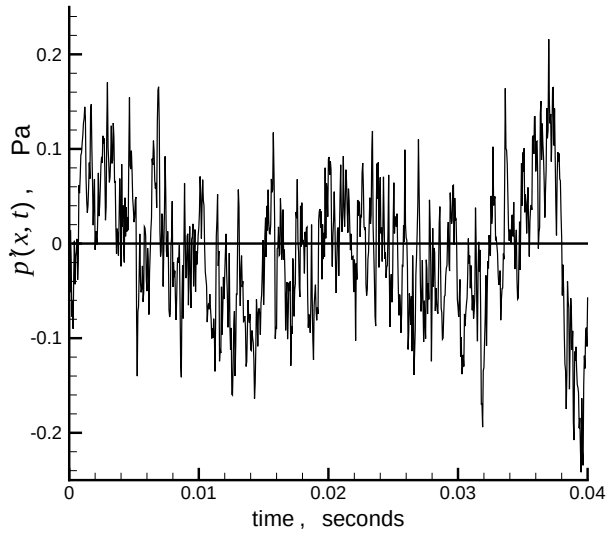

Fig. 10 Predicted far-field signal, $U = 69.5$ m/s; microphone at 90^o, 1.22 m above trailing edge.

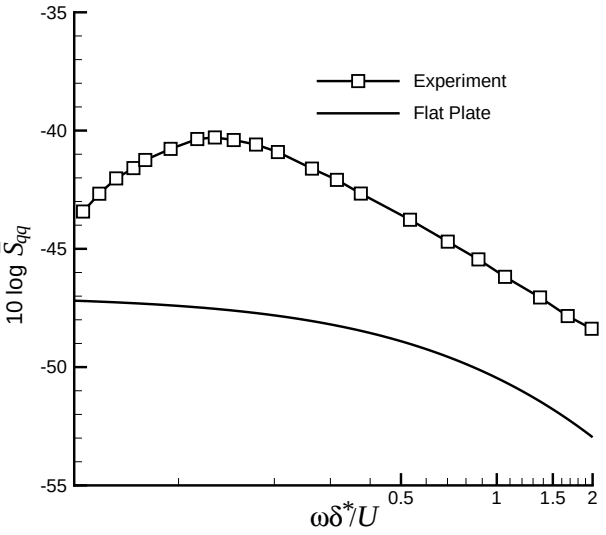

Fig. 12 Normalized surface pressure correlations; flat plate theory from Ref. 16; experimental measurements from Ref. 28.

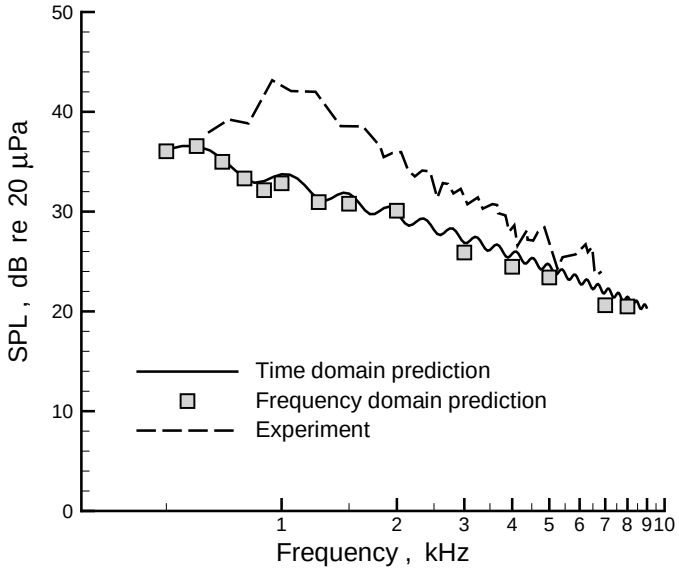

Fig. 11 Predicted and measured far field noise spectra, using surface pressure correlations from flat plate theory; $U = 69.5$ m/s; frequency domain prediction from Ref. 16; experimental data from Ref. 17.

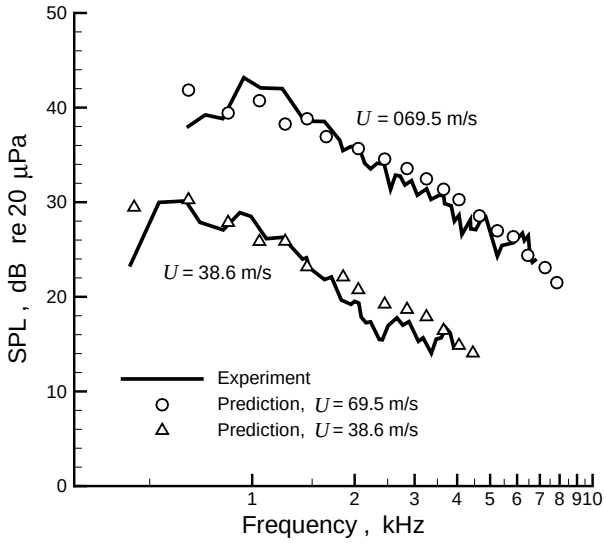

Fig. 13 Predicted and measured far-field noise spectra; predictions obtained with measured surface pressure correlations (Ref. 28); experimental SPLs from Ref. 17.